Nuclear Inst. and Methods in Physics Research B 413 (2017) 62–67

Contents lists available at ScienceDirect

Nuclear Inst. and Methods in Physics Research B

journal homepage: www.elsevier.com/locate/nimb

$In_xGa_{1-x}N$ nucleation by In+ ion implantation into GaN

C.A. Hernández-Gutiérrez[a,*], Yu. Kudriavtsev[b], Dagoberto Cardona[f], A. Guillén-Cervantes[c], G. Santana-Rodríguez[d], A. Escobosa[b], Luis Alberto Hernández-Hernández[e], M. López-López[c]

[a] Doctorado en Nanotecnologia, Cinvestav-IPN, México, DF 07360, Mexico
[b] Departamento Ingeniería Eléctrica – SEES, Cinvestav-IPN, México, DF 07360, Mexico
[c] Departamento Física, Cinvestav-IPN, México, DF 07360, Mexico
[d] Universidad Nacional Autónoma de México, Coyoacán, DF C.P. 04510, Mexico
[e] Escuela Superior de Física y Matemáticas – Instituto Politécnico Nacional, San Pedro Zacatenco, C.P. 07738 Mexico DF, Mexico
[f] Departamento de Matemáticas y Física, ITESO, Periférico Sur Manuel Gómez, Morín # 8585, C.P. 45604 Tlaquepaque, Jalisco, Mexico

ARTICLE INFO

Keywords:
In+ Ion implantation
GaN
$In_xGa_{1-x}N$

ABSTRACT

In+ ion implantation was performed into a GaN epi-layer with dose and energy of 5×10^{15} cm^{-2} and 25 keV respectively. After implantation, a thermal annealing process was employed and then the characterization was carried out by HRXRD, Raman spectroscopy, STEM, SIMS, XPS, and Photoluminescence. The maximum Indium concentration was measured by SIMS reaching to an atomic concentration of 3%. The HRXRD revealed the formation of $In_xGa_{1-x}N$ with a variable distribution of Indium due to the implantation profile. The nucleation of $In_xGa_{1-x}N$ was confirmed by the observation of interplanar spacings of 0.267 nm. The Photoluminescence analysis showed a modification of GaN spectra as a function of annealing temperature with an interesting green emission for samples annealed at 500 °C. The green emission is explained by the formation of $In_xGa_{1-x}N$ with x value as high as 0.32 within rich Indium regions.

1. Introduction

$In_xGa_{1-x}N$ is one of the most important semiconductors after Si, GaAs, and GaN due to its special properties such as tunable band gap, high absorption coefficient, resistance to high temperatures and radiation. The band gap is well established in the range from 0.7 to 3.4 eV varying the Indium concentration suitable to absorb and emit radiation [1]. $In_xGa_{1-x}N$ based devices such as LEDs, photodetectors, and solar cells have been proven [2,3]. However, technological challenges persist in obtaining high-efficiency devices. The important issues are the Indium surface segregation and the difficulty to achieve high Indium concentrations without phase separation during epitaxial growth: these results in a high surface roughness and a poor crystalline quality of epitaxial $In_xGa_{1-x}N$. Furthermore, this deterioration will become more serious as the thickness of the $In_xGa_{1-x}N$ layer is increased [4–6]. These challenges cause complex growth conditions even for epitaxial techniques such as molecular beam epitaxy (MBE) and Metal organic chemical vapor deposition (MOCVD). To incorporate more than 20% of Indium concentration with acceptable crystal and surface quality a sophisticated MBE growth process has been reported such as modulation of Gallium and Indium shutters using Metal-Modulated Epitaxy (MME) [7]. Therefore as an alternative to $In_xGa_{1-x}N$ nucleation, we propose a study of high dose and low energy In+ ion implantation into GaN. The In+ ion implantation into GaN has been performed by our group to fabricate low resistance ohmic contacts [8]. However, the effects of implantation on the GaN photoluminescence have not been reported yet. The existing reports of In+ implantation into GaN are focused on the radiation damages at different energies and doses [9,10]. In Addition, GaN and InN nanocrystals have been observed after implantation and annealing of N+ ions into GaAs or InAs respectively [11,12]. Nevertheless, to our knowledge, the $In_xGa_{1-x}N$ or InN nanocrystals have not been observed into GaN by ion implantation.

2. Experimental details

Commercial Mg-doped p-type GaN and not intentionally doped (nid) GaN templates were used in this study. We use two type of conductivity substrate to demonstrate that the implantation showed the same effect for “p” and “n” type GaN. Thus only in PL characterization, we will show the data for both substrates to demonstrate that the Mg doping does not affect the implantation conclusions. The samples were grown by metal-organic chemical vapor deposition (MOCVD) on sapphire substrates using AlN as a buffer layer.

In+ ion implantation was carried out at 25 keV and the ion dose

* Corresponding author.
E-mail address: chernandez@fis.cinvestav.mx (C.A. Hernández-Gutiérrez).

http://dx.doi.org/10.1016/j.nimb.2017.10.013
Received 26 April 2017; Received in revised form 6 September 2017; Accepted 14 October 2017
Available online 05 November 2017
0168-583X/ © 2017 Elsevier B.V. All rights reserved.

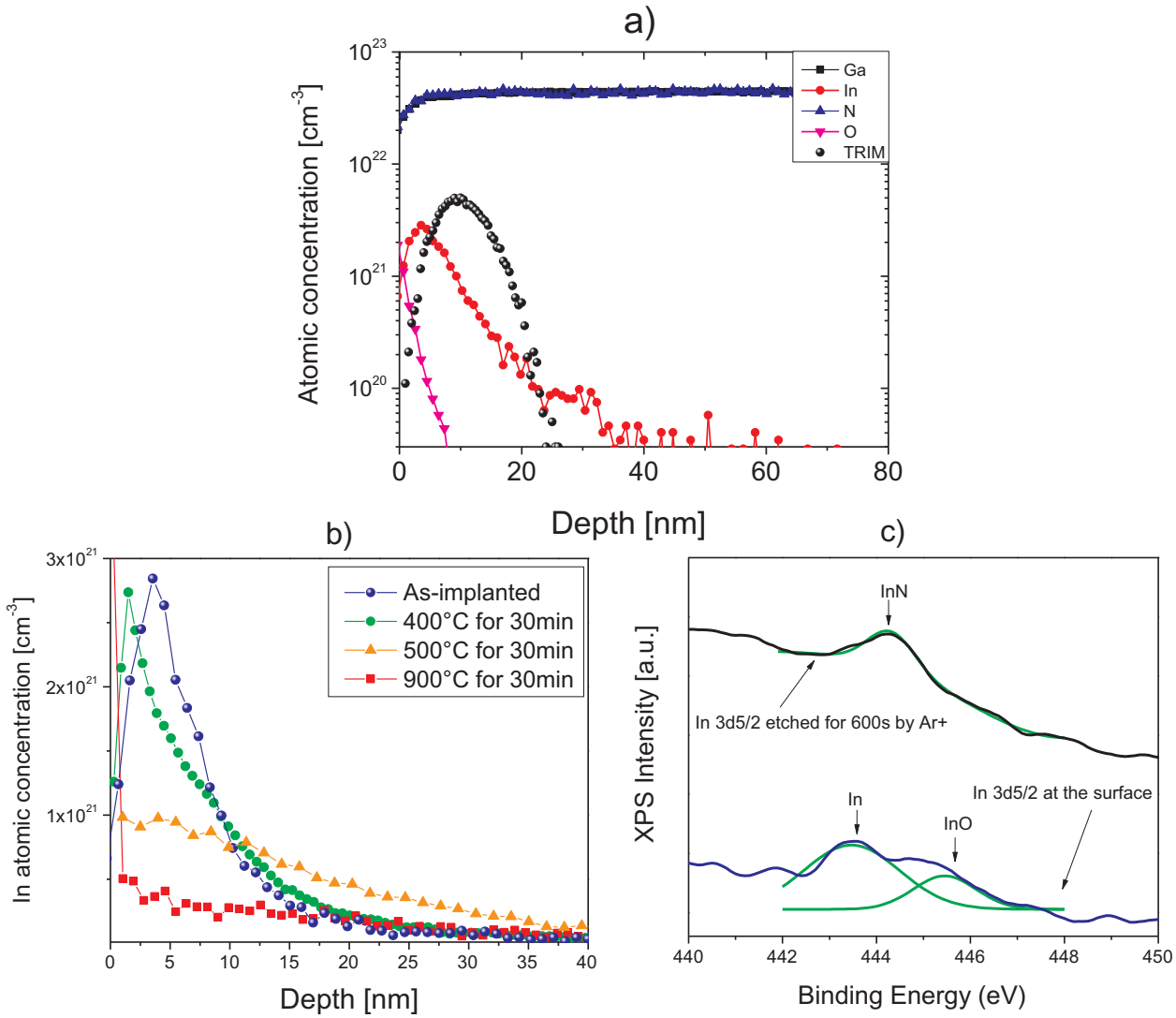

Fig. 1. SIMS (a,b) and XPS (c) analysis of the implanted sample.

was 5×10^{15} ions/cm^2. Moreover, the ion flux was performed normal to the surface of GaN at room temperature. So according to TRIM, the implantation was designed to achieve a maximum atomic concentration of Indium around 6%. After implantation, the In+ implanted wafer was cut to perform samples annealed at different temperatures. Therefore we achieved implanted and annealed samples at 400 °C, 500 °C, and 900 °C. In all annealing process, an ammonia atmosphere was employing during 30 min. To study the structural effect of the implantation into GaN, high-resolution X-ray diffraction (HRXRD) ω-2θ scan was carried out, with a scan range of 32.35°–36.34° centered over (0 0 2) plane at 34.5468° employing a high-resolution system Panalytical MRD X-ray diffractometer. To further support a set of lamellas was fabricated by a JIB-4500 MULT-IBEAM SEM-FIB using Ga+ ions obtaining a sample thickness around 50 nm. The analysis of lamellas was carried out in a 0.08 nm resolution JEM-ARM200F transmission electron microscope operated at 200 kV. Phase formation and radiation damage were monitored by Raman spectroscopy with a NTEGRA Spectra instrument from NT-MDT with a green laser emitting at 532 nm. The exposure time was 60 s and the spectra were recorded with a CCD detector cooled at 238 K using a 100× objective. Elemental depth distribution and their re-distribution after thermal annealing process were analyzed using a TOF-SIMS-5 secondary ion mass spectrometer from ION-TOF GmbH. We used a double beam analysis regime: a focused cesium ion beam with an energy of 500 eV and ion current of 60 nA was raster scanned over 500 × 500 μm^2 area and a pulsed Bi_3^+ ion beam was used to analyze a 150 × 150 μm^2 in a central area of the sputtered crater. Secondary CsM^+ cluster ions (where M is an element of interest) were monitored to minimize the SIMS matrix effect at the semiconductor interface and experimental crater depth was measured by a Dektak XT profiler.

X-ray photoelectron spectroscopy (XPS) analysis was carried out using a SPECS spectrometer with a Phoibos 100 1D DLD using a monochromatic X-ray radiation Al Kα. The elemental bulk-distribution was analyzed using the XPS technique combined with Ar+ depth profile sputtering employing 500 eV to avoid Ar+ implantation and perform a low etching rate. Finally, the Photoluminescence was carried out employing a 325 nm HeCd LASER at a low temperature of 12 K.

3. Results and discussions

3.1. Chemical analysis

The experimental depth profile of the Indium implanted GaN acquired by SIMS is observed in Fig. 1a together with TRIM simulation data. The depth scale was re-calculated after experimental crater measurement, the concentration of In was re-calculated with a Relative Sensitivity Factor, obtained by using an implanted standard. The concentration of In at the implanted maximum was found as high as ~3

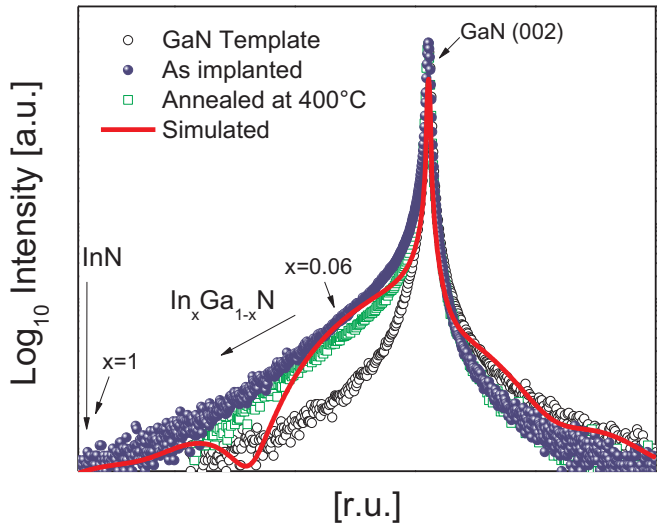

Fig. 2. HRXRD 2θ-ω analysis around (0 0 2) reflection angle in the range of GaN and $In_xGa_{1-x}N$ diffraction angles for the GaN template, As-implanted GaN and the Annealed at 400 °C.

atomic%. As it is clear from the data of TRIM simulation there is a strong sputtering effect accompanying the implantation. The sputter yield for 25 keV ion irradiation according to the TRIM reaches Y = 9.3, this suggests a few monolayers sputtering during the implantation with the fluence of 5×10^{15} ions/cm^2 used in our experiment. The experimental projected range was found as 3.6 nm, whereas TRIM predicts almost 10 nm. The sputtering effect results that the implanted dose was found as $\sim 2.4 \times 10^{15}$, or only the half of the estimated one.

Switching to the annealing discussion. SIMS reveals that after annealing, the Indium tends to diffuse to the GaN surface, moreover is observed that as the annealing temperature increased, the Indium concentration is reduced. As a result, for an annealing at 900 °C the Indium escape from GaN, see Fig. 1b.

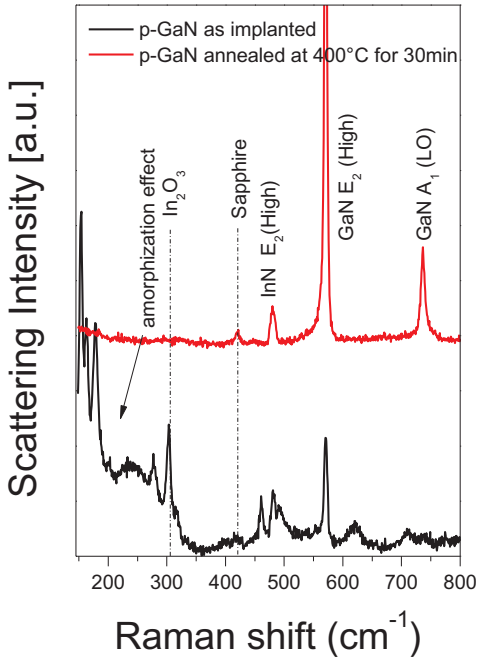

Fig. 3. Raman Shift for as-implanted and annealed at 400 °C. The black spectrum corresponds to the as-implanted sample and the red spectrum corresponds to the annealed one.

On the other hand, the XPS analysis was performed only for the as-implanted sample (see Fig. 1c). The Indium $3d_{5/2}$ binding energy was monitored, reaching to the estimated maximum atomic concentration of ~2%. The quantification of Indium atomic concentration was performed using standard sensitivity factors contained in the CasaXPS software. The XPS In $3d_{5/2}$ deconvolution analysis revealed three types of bounds, one of them is the In binding to O located at (445.5 eV) may due to the formation of In_2O_3 and also observed by Raman (see next Section 3.2), the peak around of (443.1 eV) is attributed to atomic Indium core level signal and the peak at (443.3 eV) is related to In–N bond [28]. In addition is worth to notice that at the surface we observed In–O and In signals, whereas after etching by Ar+ for 600 s at maximal Indium concentration, the In–O disappears and the signal shift to InN binding energy. Therefore from XPS InN bound was observed related with InGaN formation.

3.2. Structural analysis

3.2.1. XRD diffraction

Fig. 2 shows the simulation and experimental data of HXRD ω-2θ scan analysis over the (0 0 2) GaN crystal plane. In order to predict the effect of implantation on the structural properties, a simulation was performed using the X'pert epitaxy software. On the simulation, we considered a 20 nm of an $In_xGa_{1-x}N$ layer with a concave profile distribution of x, the maximal Indium concentration is set to be x = 0.06 just at the first 10 nm from the surface, then the Indium concentration tends to decrease reaching to GaN binary compound at the 20 nm form surface. The x = 0.06 Indium concentration in InGaN was chosen because it corresponds to a concentration of 2.84×10^{21} cm^{-3} or 3% atomic in GaN as was measured by SIMS. The simulation reveals a shoulder near the GaN peak corresponding with $In_{0.06}Ga_{0.94}N$, and then the diffraction signal starts to decrease following a concave profile. From the as-implanted sample, the analysis reveals a broad asymmetry shifted to the $In_xGa_{1-x}N$ angles reducing its diffraction intensity as the angle goes to InN diffraction angle. The sample annealed at 400 °C exhibits a similar behavior as the observed for as-implanted. Then given that the effect was found in both, for the as-implanted and annealed samples suggesting that the asymmetric should not be associated with defects caused by radiation damage. If the asymmetry had been caused by defects, the profile should be broad for both sides (toward to InN and toward to AlN), nevertheless the broad was observed only toward to InN. So, if the broad asymmetry were caused by defects it should be reduced after annealing but it was not the case. Therefore we interpreted the asymmetry as the sum of several contributions of $In_xGa_{1-x}N$ and the weak diffraction contributions are related to $In_xGa_{1-x}N$ with high Indium concentration such as x > 0.3.

3.2.2. Raman analysis

Fig. 3 shows the Raman spectra for the as-implanted and the sample annealed at 400 °C. The characteristic E2 high and LO GaN Raman peaks were clearly recognized in all cases. For the as-implanted sample, three signals have been observed, the first is a broad band in the range of 200–300 cm^{-1} attributed to the radiation damage, the second is related to In–O signal and the third is the complex 481 cm^{-1} peak which is attributed to In–N bond. After annealing the signals related to radiation damage and In–O bond were suppressed and moreover, the increase of GaN E2 high and LO signals are indicators of crystal enhancement. The complex 481 cm^{-1} peak related to InN persisted after annealing. However, the shift of the observed peak is very controversial in comparison with the well-reported InN at 488 cm^{-1} [13]. Based on Raman shift, SIMS, XPS and HRXRD, we suggest that after annealing the InN shift is due to the formation of $In_xGa_{1-x}N$ with an inhomogeneous Indium concentration.

3.2.3. STEM analysis

The STEM analysis was performed for the as-implanted sample and

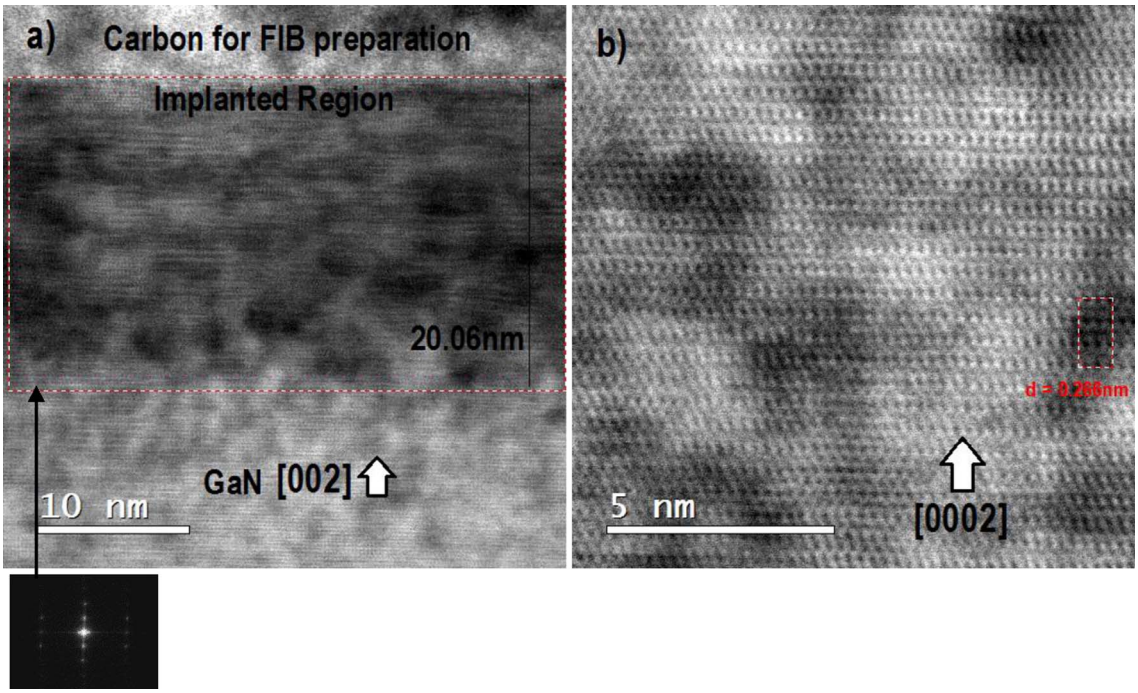

Fig. 4. As-implanted sample a) General STEM analysis and b) High-resolution STEM analysis.

the annealed at 500 °C. Fig. 4) shows the STEM analysis for the as-implanted sample while the Fig. 5) shows the analysis for the annealed at 500 °C. From the as-implanted sample, the In+ implanted zone is well recognized by the Z-contrast, the implanted zone is around 20 nm which correlates with the SIMS depth profile. The Fast Fourier Transform (FFT) was applied to the as-implanted sample and is attached to Fig. 4). The FFT reveals a remnant crystalline layer after implantation instead of the complete amorphous layer as is suggested by SRIM simulation (not shown here). To explain this discrepancy we suggest that the thermal spike regime with the formation of quenching of melting pools during 25 keV In+ ion irradiation of GaN could be considered [19–26]. On the other hand in contrast to the Lorenz et al. [27] results, they have shown that when the dose is the order of 2×10^{15} ions/cm^2 nano-crystals are formed in the GaN surface. Nevertheless to the best of our knowledge, Lorenz did not explain the formation mechanism and in addition, their employed implantation acceleration voltage was 300 keV more than 10 times greater than our employed acceleration voltage.

From the high-resolution STEM analysis of the as-implanted sample (Fig. 4b), an inhomogeneous Indium distribution within the implanted zone was observed. Then we observed that the implanted Indium tends to cluster, forming rich Indium regions which its planar spacing is around 0.266 nm. We correlated these planar spacing with the formation of (0 0 2) $In_xGa_{1-x}N$ planes.

Switching to the STEM analysis for the annealed sample at 500 °C (Fig. 5). The implanted zone presented in Fig. 5b) shows that after annealing the implanted Indium persisted instead of escaping completely from the material. High-resolution analysis within the Indium-rich regions reveals that the Indium clustering to nucleate $In_xGa_{1-x}N$ with an interplanar spacing of 0.2675 nm. Similar observations for Indium clustering have been reported for InGaN/GaN quantum wells [14,15]. According to Vegard's law, 0.2675 nm planar spacing

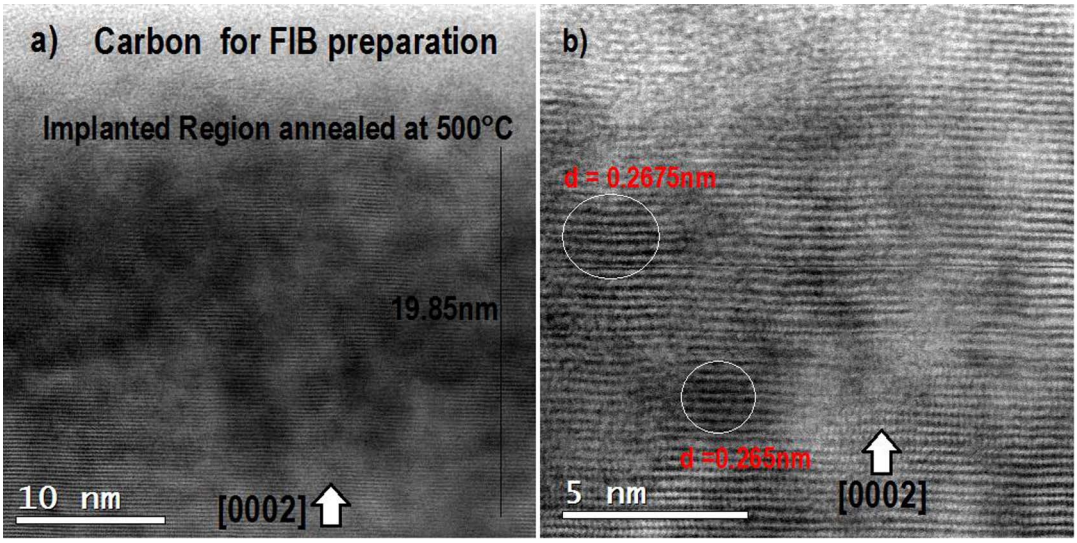

Fig. 5. Annealed sample at 500 °C, a) STEM analysis of implanted region and b) high-resolution STEM analysis. The circles are added for visual guide within rich-Indium regions.

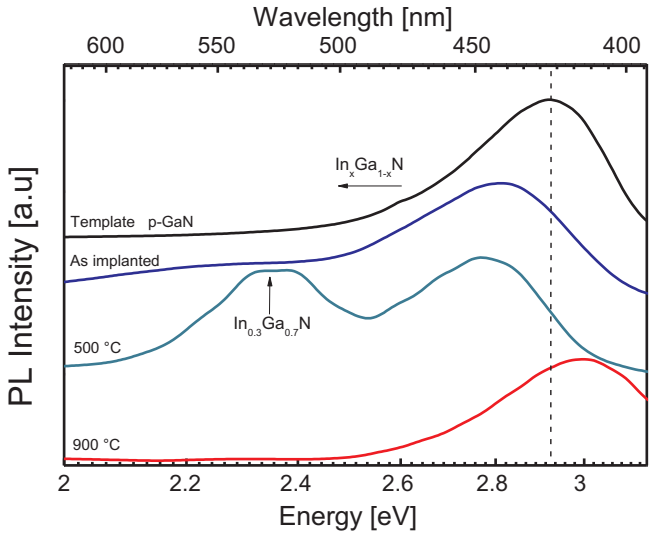

Fig. 6. 1016000107315 PL spectra of In+ implanted samples as a function of annealing temperature for GaN: Mg in comparison with not implanted or as-grown template. The arrow in the sample annealed at 500 °C indicates to the formation of $In_xGa_{1-x}N$ with a x ~ 0.32. Moreover, the PL emissions were shifted to each other in a stack for better visibility.

corresponds to an $In_{0.327}Ga_{0.673}N$ ternary alloy. Therefore based on our experimental results we suggest that within rich Indium regions, unstressed $In_xGa_{1-x}N$ with an Indium concentration x > 0.3 can be formed due to phase separation. Similar observations have been reported for $In_xGa_{1-x}N$ layers grown with a low Indium concentration in the range of (9–20%) [6,16].

3.3. Photoluminescence

To study the effect of Indium implantation into GaN, low-temperature photoluminescence was performed. Fig. 6 shows the PL spectra of the as-implanted, annealed at 500 °C, annealed at 900 °C and for comparison proposes as-grown GaN template is also included. Moreover is worth to mention that in Fig. 6 only the Mg-doped GaN samples were studied.

From Fig. 6 the p-GaN template shows its characteristic peak at around 3 eV due to the Mg deep level. The as-implanted sample presents an interesting asymmetric broad red-shift. The red shift can be explained by the formation of $In_xGa_{1-x}N$ with variable concentration as was observed by HRXRD. Then the sample annealed at 500 °C presents

Table 1
Summary of the interplanar spacing measured by STEM, Indium concentration estimated by the Vegard's law, and its corresponding band gap calculated employing the Eq. (1).

Interplanar spacing measured by STEM analysis (nm)	x Indium concentration using Vegard's law (%)	Related band gap applying the Eq. (1) (eV)
0.266	29	2.32
0.2675	32.5	2.2

two broad peaks centered at 2.7 eV and 2.3 eV. Based on our STEM results we suggest that the green emission corresponds to $In_xGa_{1-x}N$ regions with Indium concentration around 32%. In addition according to the literature, 500 °C is a suitable temperature to achieve $In_xGa_{1-x}N$ because several reports for MOCVD and MBE have shown the growth of $In_xGa_{1-x}N$ in the range of 450–600 °C [7,17]. Finally, from sample annealed at 900 °C, no emission below the band gap was observed which is due to the Indium escape out from the material as was shown in Fig. 1b). Moreover, a blue shift was observed, we suggest that it can come from donor impurity incorporation such as Carbon during the thermal annealing. However further work should be realized in future to explain the nature of the blue shift.

To demonstrate that the interesting effect of implantation into GaN is independent of the substrate conductivity. We first pointed out that the atomic Mg concentration in GaN is $\sim 7 \times 10^{19}\ cm^{-3}$ and typically the Mg deep level is ~200 meV above of valence band. In addition, the well-known yellow band is typically not observed in GaN: Mg. By another hand, the yellow band is typically observed on "n" or nid-GaN. So to demonstrate that the green emissions are not related to Mg or yellow band emission, a comparative PL study of two types of conductivity was performed. Fig. 7 illustrates the PL analysis for the samples annealed at 500 °C for both Mg-doped GaN and nid-GaN. Deconvolution analysis reveals a set of multi-peaks contributions due to the formation of several $In_xGa_{1-x}N$ ternary alloys with a no homogeneous distribution as was mentioned above. From nid-GaN spectra, the 3.4 eV excitonic GaN peak was not observed as a result of the formation of $In_xGa_{1-x}N$. It means that the In+ implanted and annealed GaN has a strong absorption coefficient and the light interaction acts only in this implanted region. So if the green emission were caused by ion implantation damage, it should be reduced by the annealing process. However, the green emission only appears after annealing. Therefore the green emission observed for both nid-GaN and GaN: Mg is not due to the yellow band or Mg deep levels.

Finally to further support of our discussions we consistently integrate the STEM planar spacing and PL emission energies by the

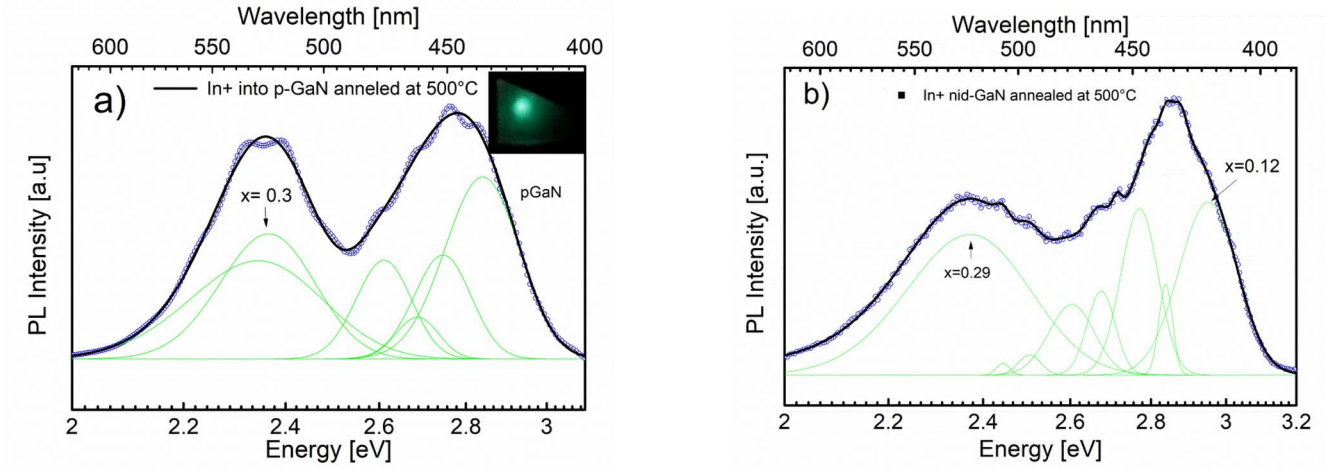

Fig. 7. PL spectra of a) GaN: Mg and b) nid-GaN implanted and annealed at 500 °C. Is worth to pointed that the green emission is observed in both substrates and in the inset of the a) demonstrates the visible green emission.

calculation of the energy gap as a function of indium content employing the bowing parameter reported in reference [18]. So the indium concentration was calculated applying the Vegard's law to the measured STEM interplanar spacing. This approach is in good correlation with our results and explains the interesting emissions. Table 1 is a summary of the interplanar spacing, related Indium concentration, and its corresponding band gap, calculated using the Eq. (1).

$$Eg = 0.7x + 3.4(1-x) - 1.43x(1-x) \quad (1)$$

4. Conclusions

In+ ion implantation was carried out at 25 keV with a dose of 5×10^{15} ions/cm^2 at room temperature into Mg-doped and nid-GaN templates, as a result, we demonstrated that the implantation effect is independent of the substrate conductivity. The crystalline structure for the as-implanted and after thermal annealing confirmed by Raman, HRXRD, and STEM, let us suggest that the thermal spike regime with the formation of quenching of melting pools during 25 keV In+ ion irradiation of GaN should be considered. After implantation and annealing at 500 °C, an interesting green emission was observed. The structural characterization by HRXRD revealed the formation of $In_xGa_{1-x}N$ with a variable Indium concentrations and STEM confirmed an Indium inhomogeneity forming $In_xGa_{1-x}N$ with a high In concentration as high as 32% within rich indium regions corresponding with interplanar spacings of ~0.2675 nm. Therefore the green emission was explained consistently by the nucleation of the $In_{0.327}Ga_{0.673}N$ ternary alloy according to XPS, HRXRD, Raman, and STEM. Finally is important to highlight that the green emission by In+ implantation has been observed for the first time in this work and can be used to absorb or emit green radiation in future applications.

Acknowledgements

We want to thanks to Consejo Nacional de Ciencia y tecnología (CONACYT) for their financial support. We also want to thanks to Dr. Daniel Bahena Uribe, Alvaro Angeles Pascual, Adolfo Tavira Fuentes, Georgina Ramírez Cruz, Ruben Montelongo, the LANE laboratory and the ITESO nanotechnology laboratory for their technical support.

References

[1] J. Wu, W. Walukiewicz, K. Yu, W. Shan, J. Ager Iii, E. Haller, H. Lu, W.J. Schaff, W. Metzger, S. Kurtz, Superior radiation resistance of In 1−x Ga x N alloys: full-solar-spectrum photovoltaic material system, J. Appl. Phys. 94 (10) (2003) 6477–6482.
[2] Hongjian Li, Panpan Li, Junjie Kang, Jiianfeng Ding, Jun Ma, Yiyun Zhang, Xiaoyan Yi, Guohong Wang, Broadband full-color monolithic InGaN light-emitting diodes by selfassembled InGaN quantum dots, Sci. Rep. 6 (35217) (2016) 1–7.
[3] S. Valdueza-Felip, A. Ajay, L. Redaelli, M.P. Chauvat, P. Ruterana, T. Cremel, M. Jiménez-Rodríguez, K. Kheng, E. Monroy, P-i-n InGaN homojunctions (10–40% In) synthesized by plasma-assisted molecular beam epitaxy with extended photoresponse to 600 nm, Appl. Phys. Lett. 76 (2000) 2728–2730.
[4] J. Wu, When group-III nitrides go infrared: new properties and perspectives, J. Appl. Phys. 106 (Jul. 2009) 011101.
[5] A. Yamamoto, M.R. Islam, T.-T. Kang, A. Hashimoto, Recent advances in InN-based solar cells: status and challenges in InGaN and InAlN solar cells, Phys. Status Solidi C 7 (5) (Mar. 2010) 1309–1316.
[6] F.A. Ponce, et al., Microstructure and electronic properties of InGaN alloys, Phys. Status Solidi B 240 (2) (Nov. 2003) 273–284.
[7] Michael Moseley, Brendan Gunning, Jordan Greenlee, Jonathan Lowder, Gon Namkoong, W. Alan Doolittle, Observation and control of the surface kinetics of InGaN for the elimination of phase separation, J. Appl. Phys. 112 (2012) 014909.
[8] C.A. Hernández-Gutierrez, Yu. Kudriavtsev, Esteban Mota, A.G. Hernández, A. Escobosa-Echavarría, V. Sánchez-Resendiz, Y.L. Casallas-Moreno, M. López-López, A new method of making ohmic contacts to p-GaN, Nucl. Instrum. Methods B 388 (2016) 35–40.
[9] M. Katsikini, J. Arvanitidis2, S. Ves, E.C. Paloura, E. Wendler, W. Wesch, Indium implantation and annealing of GaN: lattice damage and recovery, Phys. Status Solidi C 7 (1) (2010) 36–39.
[10] M. Katsikini, F. Pinakidou, E.C. Paloura, E. Wendler, W. Wesch, R. Manzke, N – K edge NEXAFS study of the defects induced by indium implantation in GaN, J. Phys. Conf. Ser. 190 (2009) 012065.
[11] A.W. Wood, R.R. Collino, P.T. Wang, Y.Q. Wang, R.S. Goldman, Formation and transformation of embedded GaN nanocrystals, Appl. Phys. Lett. 100 (2012) 203113.
[12] A.W. Wood, X. Weng, Y.Q. Wang, R.S. Goldman, Formation mechanisms of embedded wurtzite and zincblende indium nitride nanocrystals, Appl. Phys. Lett. 99 (2011) 093108.
[13] O. Briot, B. Maleyre, S. Ruffenach, B. Gil, C. Pinquier, F. Demangeot, J. Frandon, Absorption and Raman scattering processes in InN films and dots, J. Cryst. Growth 269 (2004) 22–28.
[14] H.K. Cho, J.Y. Lee, N. Sharma, C.J. Humphreys, G.M. Yang, C.S. Kim, J.H. Song, P.W. Yu, Effect of growth interruptions on the light emission and indium clustering of InGaN/GaN multiple quantum wells, Appl. Phys. Lett 79 (2001) 2594.
[15] T.M. Smeeton, M.J. Kappers, J.S. Barnard, M.E. Vickers, C.J. Humphreys, Electron-beam-induced strain within InGaN quantum wells: false indium "cluster" detection in the transmission electron microscope, Appl. Phys. Lett. 83 (2003) 5419.
[16] D. Gerthsen, E. Hahn, B. Neubauer, A. Rosenauer, O. Schon, M. Heuken, A. Rizzi, Composition fluctuations in InGaN analyzed by transmission electron microscopy, Phys. Status Solidi A 177 (145) (2000).
[17] Zhen Bi, Jincheng Zhang, Qiye Zheng, Ling Lv, Zhiyu Lin, Hengsheng Shan, Peixian Li, Xiaohua Ma, Yiping Han, Yue Hao, An InGaN-based solar cell including dual InGaN/GaN multiple quantum wells, IEEE Photonics Technol. Lett 28 (20) (2016).
[18] J. Wu, W. Walukiewicz, K.M. Yu, J.W. Ager III, E.E. Haller, Lu Hai, William J. Schaff, Small band gap bowing in In1-xGaxN alloys, Appl. Phys. Lett. 80 (2002) 25.
[19] S.O. Kucheyev, J.S. Williams, S.J. Pearton, Ion implantation into GaN, Mater. Sci. Eng. 33 (2001) 51–107.
[20] T. Diaz de la Rubia, R.S. Averback, R. Benedek, W.E. King, Role of thermal spikes in energetic displacement cascades, Phys. Rev. Lett. 59 (1987) 1930.
[21] T. Diaz de la Rubia, R.S. Averback, H. Hsieh, R.S. Benedek, Molecular dynamics simulation of displacement cascades in Cu and Ni: thermal spike behavior, J. Mater. Res. 4 (1989) 579.
[22] G.H. Kinchin, R.S. Pease, Rep. Progr. Phys. 18 (1955) 1.
[23] H. Gnaser, Low-energy ion irradiation of solid surfaces, Springer Verlag, Berlin, 1999, p. 13.
[24] L. Bischoff, K.H. Heinig, B. Schmidt, S. Facsko, W. Pilz, Self-organization of Ge nanopattern under erosion with heavy Bi monomer and cluster ions, Nucl. Instrum. Methods, B 272 (198) (2012).
[25] A.G. Hernández, Yu. Kudriavtsev, Bim+ ion beam patterning of germanium surfaces at different temperatures and ion fluence, J. Vac. Sci. Technol., B 34 (2016) 061805.
[26] O. El-Atwani, S.A. Norris, K. Ludwig, S. Gonderman, J.P. Allain, Ion beam nanopatterning of III-V semiconductors: consistency of experimental and simulation trends within a chemistry-driven theory, Sci. Rep. 5 (2015) 18207.
[27] Pierre Ruterana, Marie-Pierre Chauvat, Katharina Lorenz, Mechanisms of damage formation during rare earth ion implantation in nitride semiconductors, Jpn. J. Appl. Phys. 52 (2013) 11NH02.
[28] K. Li, A.T.S. Wee, J. Lin, Z.C. Feng, S.J. Chua, X-Ray photoelectron spectroscopy evaluation on surface chemical states of Gan, Ingan and Aigan heteroepitaxial thin films grown on sapphire by mocvd, Mater. Res. Soc. Symp. Proc. 618 (2000).